






Research Article

Detection of radio emission from stars via proper-motion searches

Laura N. Driessen^{1,2}, George Heald², Stefan W. Duchesne², Tara Murphy^{1,3}, Emil Lenc⁴, James K. Leung^{1,4,3}, and Vanessa A. Moss^{4,1}

¹Sydney Institute for Astronomy, School of Physics, University of Sydney, Camperdown, NSW 2006, Australia, ²CSIRO, Space and Astronomy, PO Box 1130, Bentley, WA 6102, Australia, ³ARC Centre of Excellence for Gravitational Wave Discovery (OzGrav), Hawthorn, Victoria, Australia and ⁴CSIRO, Space and Astronomy, PO Box 76, Epping, NSW 1710, Australia

Abstract

We present a method for identifying radio stellar sources using their proper-motion. We demonstrate this method using the FIRST, VLASS, RACS-low and RACS-mid radio surveys, and astrometric information from *Gaia* Data Release 3. We find eight stellar radio sources using this method, two of which have not previously been identified in the literature as radio stars. We determine that this method probes distances of ~ 90 pc when we use FIRST and RACS-mid, and ~ 250 pc when we use FIRST and VLASS. We investigate the time baselines required by current and future radio sky surveys to detect the eight sources we found, with the SKA (6.7 GHz) requiring < 3 yr between observations to find all eight sources. We also identify nine previously known and 43 candidate variable radio stellar sources that are detected in FIRST (1.4 GHz) but are not detected in RACS-mid (1.37 GHz). This shows that many stellar radio sources are variable, and that surveys with multiple epochs can detect a more complete sample of stellar radio sources.

Keywords: radio astrometry – radio continuum emission – Galactic radio sources – proper motions – stellar flares

(Received 25 October 2022; revised 4 May 2023; accepted 8 May 2023)

1. Introduction

A recent large increase in the sample of known radio stars (see e.g. Wendker 1995, for a catalogue of stellar radio sources) has been enabled by the advent of wide-field of view, high-resolution interferometers such as the Karl G. Jansky Very Large Array (VLA; Perley et al. 2011), the Low Frequency Array (LOFAR; van Haarlem et al. 2013), the Australian Square Kilometre Array Pathfinder (ASKAP^a; Hotan et al. 2021) and the (more) Karoo Array Telescope (MeerKAT; Camilo et al. 2018). New radio stars have been identified using circular polarisation searches (e.g. Pritchard et al. 2021; Callingham et al. 2021a; Toet et al. 2021), and variability searches (e.g. Driessen et al. 2020; Driessen et al. 2022; Andersson et al. 2022). Finding radio stars is important for probing the physics behind stellar radio emission, for searching for radio signatures of exoplanets (Bower et al. 2009; Curiel et al. 2020), and for tying optical and radio reference frames together. As we use current instruments and look forward to the SKA, we need to consider new methods for searching for and confirming the detection of radio emission from stellar sources.

The key challenge of identifying stellar radio emission is chance coincidence with background radio galaxies. Direct position matches between the optical and radio result in high chance coincidence probability (Callingham et al. 2019) unless the samples are first restricted using the physical properties of the radio and/or optical sources. For example, both ASKAP

and LOFAR have been used to perform circular polarisation searches for stellar sources (e.g. Pritchard et al. 2021; Callingham et al. 2021a; Toet et al. 2021). In the radio sky, only pulsars and stellar radio sources are known to have high circular polarisation fractions, and the sky density of highly circularly polarised sources is low. This reduces the chance coincidence probability and provides a physical reason to believe that a match between a highly circularly polarised radio source and an optical star is true. This has been demonstrated with great success by Pritchard et al. (2021) using ASKAP where they identified 10 known and 23 previously unknown radio stars, and by Callingham et al. (2021a) and Toet et al. (2021) using LOFAR where they detected 1 known and 18 previously unknown active stars, and 14 known RS Canum Venaticorum (RS CVn) respectively. Highly circularly polarised stellar emission is typically coherent and non-thermal, caused by either plasma emission or electron-cyclotron maser emission (see e.g. Dulk 1985, for a review of stellar radio emission mechanisms). This means that circular polarisation searches are biased towards coherent emission processes.

Stellar systems are known to flare in the radio on typical time scales of minutes to hours (see Osten 2008, for a summary), which means stellar systems can be found in radio variability searches. All searches for radio stars are biased towards stars that flare more often as we are more likely to detect such stars. This is particularly the case for the MeerKAT results due to the serendipitous nature of the discoveries in variability searches (Driessen et al. 2020, 2022; Andersson et al. 2022). A search method that does not rely on high circular polarisation fraction and can be used for both quiescent and flaring stars would reduce the current biases in searches for radio emission from stellar sources.

Very-Long Baseline Interferometry (VLBI) of stellar radio sources has been used in the past to perform high-precision radio

Corresponding author: L. N. Driessen; Email: Laura@Driessen.net.au.

Cite this article: Driessen LN, Heald G, Duchesne SW, Murphy T, Lenc E, Leung JK and Moss VA. (2023) Detection of radio emission from stars via proper-motion searches. *Publications of the Astronomical Society of Australia* 40, e036, 1–17. <https://doi.org/10.1017/pasa.2023.26>

^a<https://www.atnf.csiro.au/projects/askap/index.html>.

Table 1. Survey information for FIRST, RACS-mid, RACS-low and VLASS. The total number of sources includes all of the sources without any cuts applied; except for VLASS, which has been restricted to sources where the MainSample flag = 1. The integration time is the typical time per pointing. As VLASS is observed ‘on the fly’, it does not have a typical integration time. Instead, VLASS was observed at a rate of approximately 23.83 arcmin h⁻¹ (Lacy *et al.* 2020).

Survey	Frequency range (MHz)	Earliest epoch	Latest epoch	Typical RMS (mJy beam ⁻¹)	Number of sources	Position accuracy (″)	Declination range	Integration time (s)
FIRST	1 354.5–1 445.5	J1993.207	J2011.312	0.2	946 432	1.0	>−11.5°	180
RACS-low	743.5–1 031.5	J2019.302	J2020.472	0.27	2 665 933	~2.0	<30°	900
RACS-mid	1 295.5–1 439.5	J2020.969	J2022.173	0.2	4 944 458	~2.0	<45°	900
VLASS	2 000–4 000	J2017.685	J2019.539	0.13	1 880 195	0.5	>−20°	

astrometry. This has been done for various reasons including: astrometric monitoring to search for signatures of orbiting exoplanets (e.g. Lestrade *et al.* 1994; Jones *et al.* 1995), to link optical and radio reference frames (e.g. Lestrade *et al.* 1988, 1999), and to distinguish between background galaxies and foreground radio stars using the stars’ proper-motion (Lestrade *et al.* 1992). However, searching for proper-motion radio stars has not previously been expanded to large-scale radio surveys. We now have long time baselines between the VLA Faint Images of the Radio Sky at Twenty-centimetres (FIRST; Becker, White, & Helfand 1994, 1995, performed between 1993 and 2011), the VLA Sky Survey (VLASS; Gordon *et al.* 2021, performed between 2017 and 2019), and the Rapid ASKAP Continuum Survey (RACS^b) at 887.5 MHz (RACS-low; McConnell *et al.* 2020; Hale *et al.* 2021, performed between 2019 and 2020), and at 1 367.5 MHz (RACS-mid; Duchesne *et al.* submitted, performed between 2020 and 2022). We also have high-precision proper-motion measurements from Gaia Data Release 3 (DR3; Gaia Collaboration *et al.* 2016; Babusiaux *et al.* 2022; Vallenari *et al.* 2022) We can now combine these surveys to search for radio stars using their proper-motion.

We have performed a search for stellar radio sources using the FIRST, VLASS, RACS-low, and RACS-mid radio surveys and the proper-motion properties of optical sources from *Gaia* DR3. In Section 2 we present the search method. In Section 3 we present the results of using the method with FIRST, VLASS and RACS. In Section 4 we present a search for candidate variable radio stellar sources. In Sections 5 and 6 we discuss the results and conclude.

2. Method

We used the proper-motion information from *Gaia* DR3 and the position of radio sources in FIRST, VLASS, RACS-low and RACS-mid to search for radio stars.

The FIRST survey was performed using the VLA in B-configuration at 1 400 MHz between 1993 and 2011. It covers over 10 000 square degrees and has a minimum declination of ~−10°. It has an astrometric accuracy of 1″ and a typical root-mean-square (RMS) noise of ~0.2 mJy (Becker *et al.* 1994). VLASS was performed using the VLA in B- and BnA-configuration at 2 000–4 000 MHz between 2017 and 2019. It covers the entire sky above a declination of ~−40°. It has an astrometric accuracy of 0.5″ above ~−20°. Epoch 1.1 of VLASS has a typical RMS noise of 128 μ Jy beam⁻¹ and epoch 1.2 has a typical RMS noise of 145

μ Jy beam⁻¹. RACS was performed using the 36-antenna ASKAP telescope with as many antennas as available at any given point. RACS-low was observed at 887.5 MHz between 2019 and 2020 and RACS-mid was observed at 1 367.5 MHz between 2020 and 2022. Both RACS surveys have an astrometric accuracy of 2″. RACS-low and RACS-mid have median RMS noise across all tiles of ~0.27 and ~0.20 mJy beam⁻¹ respectively. We create a simple, alternate catalogue for RACS-mid by concatenating source-lists from the individual RACS-mid images. Relevant metadata, such as observation start time, are added to each source entry during this process. There are a total of 4 944 458 sources in the concatenated catalogue. As each RACS-mid observation overlaps with adjacent observations to provide uniform sensitivity over the full survey, there are \gtrsim 700 000 sources recorded more than once. A summary of the radio survey details is shown in Table 1. *Gaia* is a European Space Agency (ESA) space observatory that has been designed to measure precise positions, distances and proper-motions of optical sources. The third data release was made available on 2022 June 13 and contains astrometric information (and more) for $\sim 1.46 \times 10^9$ sources.

To perform the proper-motion matching, we determined the positions at epoch A and epoch B of an optical source that has a proper-motion. If the epoch A position of the optical source matched the position of a radio source from Survey A observed on epoch A, and the epoch B position of the optical source matched the position of a radio source from Survey B observed on epoch B, then the optical source is the radio source. There are some caveats to this simple matching.

We assumed that we had two radio surveys, survey A and survey B, where survey A has position accuracy a'' and is earlier (epoch A) than survey B (epoch B) with position accuracy b'' , illustrated in Figure 1. We defined the requirements for a proper-motion match between source A from survey A and source B from survey B to be:

1. both source A and source B have $F_{\text{int}}/F_{\text{peak}} \leq 1.5$ where F_{int} and F_{peak} are the integrated and peak flux densities respectively
2. source A is separated by $D_{R_A, R_B} > a'' + b''$ from any and all survey B sources
3. source B is separated by $D_{R_A, R_B} > a'' + b''$ from any and all survey A sources
4. the source A position and the *Gaia* position proper-motion corrected to epoch A are separated by $D_{G_A, R_A} < a''$
5. the source B position and the *Gaia* position proper-motion corrected to epoch B are separated by $D_{G_B, R_B} < b''$

^bASKAP data, including the RACS-low and RACS-mid data (DOI: <https://doi.org/10.25919/1khs-c716>), are publicly available and can be accessed via the CSIRO ASKAP Science Data Archive (CASDA): <https://research.csiro.au/casda/>.

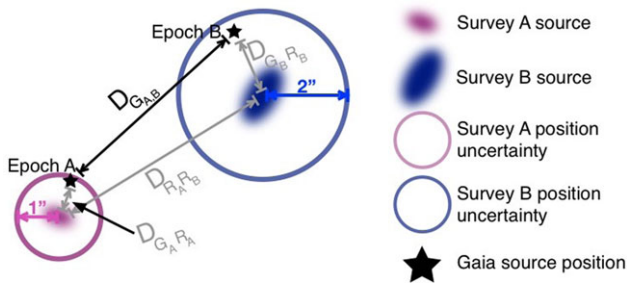


Figure 1. Diagram showing the definitions of the separations between the radio and *Gaia* positions. We will be discussing positions and separations in different epochs and comparing radio and optical positions. In this diagram we define: $D_{G_A, B}$ as the separation between the *Gaia* position proper-motion corrected to epoch A (G_A) and the *Gaia* position proper-motion corrected to epoch B (G_B); D_{R_A, R_B} as the separation between the survey A radio source position (R_A) and the survey B radio source position (R_B); D_{G_A, R_A} as the separation between the *Gaia* position proper-motion corrected to epoch A and the survey A radio position; and D_{G_B, R_B} as the separation between the *Gaia* position proper-motion corrected to epoch B and the survey B radio position.

6. the survey A position and the *Gaia* position proper-motion corrected to epoch B are separated by $D_{G_B, R_A} > a''$
7. the survey B position and the *Gaia* position proper-motion corrected to epoch A are separated by $D_{G_A, R_B} > b''$

Requirement 1 is to remove resolved sources from the set of survey A and B sources. Requirements 2, 3, 6 and 7 are to ensure that the radio source is associated with the optical high-proper-motion object, instead of a background source that does not have a proper-motion. A diagram illustrating which radio sources would be removed to satisfy requirements 2 and 3 is shown in Figure 2. Requirements 4 and 5 ensure that the radio sources match the proper-motion source.

Practically, satisfying some of these requirements ensured that others are satisfied. First, we discarded the survey A and B sources where $F_{int}/F_{peak} \geq 1.5$ to satisfy requirement 1. If we found the separation between the remaining sources in survey A and survey B and removed sources in survey A that are $D_{R_A, R_B} < a'' + b''$ from a survey B source and vice versa, we satisfied requirements 2 and 3. If we proper-motion corrected the *Gaia* positions and matched them to survey A and discarded the *Gaia* sources where the separation is $> a''$, we satisfied 4. If we then proper-motion corrected the remaining *Gaia* sources with survey B and discarded *Gaia* sources where the separation is $> b''$, we satisfied requirement 5. The remaining *Gaia* sources necessarily satisfied requirements 6–7 as the survey A and B sources they were matched to are separated by $> a'' + b''$. This means that our steps were as follows:

1. Discard *Gaia* sources that have no measured proper-motion magnitude
2. Discard sources in survey A and survey B where $F_{int}/F_{peak} > 1.5$
3. Keep any A sources that are separated by $> a'' + b''$ from all B sources and keep any B sources that are separated by $> a'' + b''$ from all A sources
4. Proper-motion correct the *Gaia* source positions to the survey A epoch and cross-match the source positions. The sources are considered a match if the separation is $< a''$. Discard those *Gaia* and survey A sources that do not match.

5. Proper-motion correct the remaining *Gaia* source positions to the survey B epoch and cross-match the source positions. The sources are considered a match if the separation is $< b''$. Discard those *Gaia* (and the corresponding survey A sources) and survey B sources that do not match.

The remaining survey A, survey B and *Gaia* sources were considered proper-motion matches, a diagram demonstrating a *Gaia* source that meets our requirements is shown in Figure 3. We then manually examined the radio sources in the images to confirm the results and to confirm that the radio sources are unresolved.

We used FIRST as the oldest survey/survey A in all cases, and matched to each of VLASS, RACS-low and RACS-mid. We used FIRST as it covers a large area of sky and has good position accuracy ($\sim 1''$ for point sources). RACS-low and RACS-mid are the first southern hemisphere all-sky surveys with position accuracy ($\sim 2''$) comparable to FIRST. Both RACS surveys and VLASS were performed $\gtrsim 25$ yr after the first FIRST observations, providing an excellent time baseline, which meant that we could search for optical sources with lower proper-motions. The position accuracy, RMS noise level, declination range, number of sources and observing epoch ranges for FIRST, VLASS, RACS-low and RACS-mid are shown in Table 1. We note that these surveys are not performed at the same frequencies. We therefore assumed that the stellar sources have close-to flat radio spectra. As per the VLASS quick look catalogue paper suggestions (Gordon et al. 2021), we used the sources where the MainSample (or e.1) flag is 1. This meant that only sources with declination $> -20^\circ$ were included.

3. Results

We performed the matches using the radio position accuracies shown in Table 1 as the required separations for each survey. We found eight unique stars, seven stars using FIRST and VLASS, six stars using FIRST and RACS-mid, and none using FIRST and RACS-low. This is likely because of higher noise in some RACS-low pointings and because the RACS-low catalogue convolved all of the images to the common resolution. There are 5 stars common to both VLASS and RACS-mid. The positions of the stars in the various epochs and the separation between the source positions after proper-motion correction are shown in Table 2 and the radio images are shown in Figure 4. We can see in the table the sources that are detected in more than one survey. The flux densities of the sources from the radio surveys are shown in Table 3, this includes sources that were not found in RACS-mid using the proper-motion method but do have a RACS-mid detection. Here we will discuss each of the eight stars found using proper-motion searching. PM J15587+2351E has not previously been identified as a radio star. It is an M5e D type M dwarf star (e.g. Cook et al. 2016; Bowler et al. 2019) and is 35.4 ± 0.1 pc away (Bailer-Jones et al. 2021).

GS Leo has not previously been identified as a radio star. It is a known X-ray star and is known to be variable. GS Leo is a tight 3.5 d G9V+K4 binary in a wide binary with a K0 star (e.g. Strassmeier et al. 2012; Samus' et al. 2017) that is 35.37 ± 0.04 pc away (Bailer-Jones et al. 2021).

σ Coronae Borealis (sig CrB) A has previously been detected in the radio using VLBI to discern the stellar radio emission from a nearby QSO (Lestrade et al. 1992). Similar to our method, they used the proper-motion to determine that the radio emission is moving across the sky. σ CrB A has recently been detected at

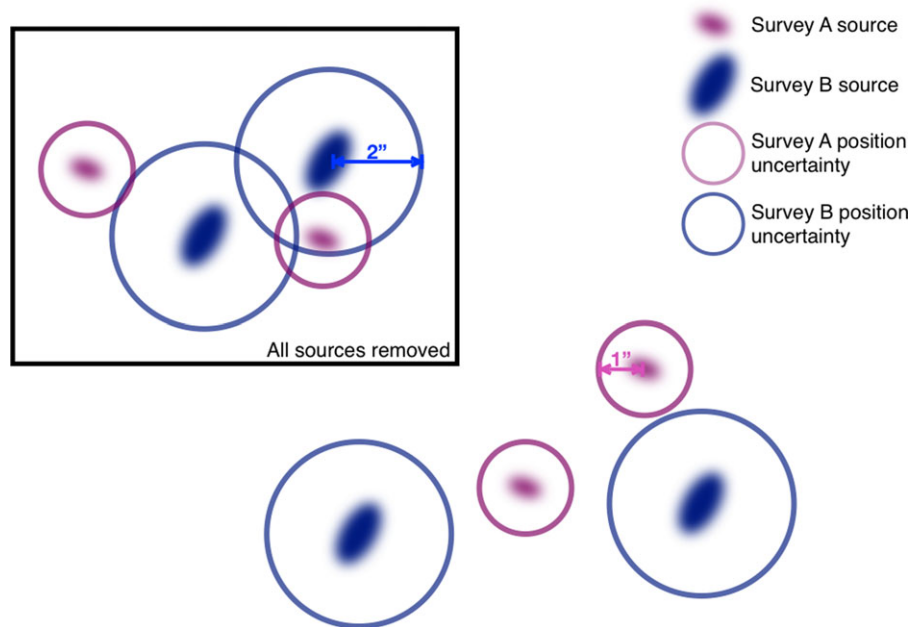


Figure 2. Diagram illustrating which radio sources are kept and which radio sources are removed to satisfy requirements 2 and 3. All of the sources from both surveys within the black box are discarded while the sources outside of the box are kept.

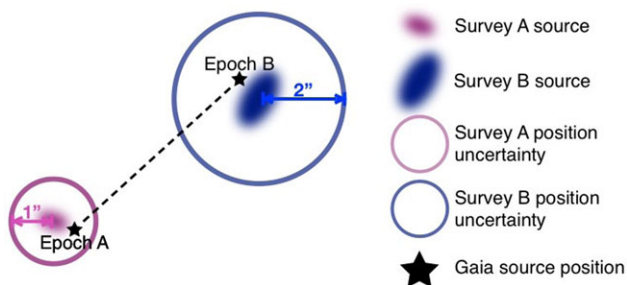


Figure 3. Diagram demonstrating a *Gaia* source that would be considered a radio proper-motion source. The black star indicates the position of the same *Gaia* source in the two different radio survey epochs.

144 MHz in both Stokes I and Stokes V using LOFAR (Toet *et al.* 2021). It is a spectroscopic, RS CVn binary and is $22.68^{+0.03}_{-0.02}$ pc away (Bailer-Jones *et al.* 2021).

σ Gemini (sig Gem) is a known FIRST radio star and it has been detected by LOFAR in Stokes I at 144 MHz (Vedantham *et al.* 2022). Spangler, Owen, & Hulse (1977) made the first tentative radio detection. It is an RS CVn type binary with a K1III component (e.g. Kervella *et al.* 2019) and is 36.9 ± 0.5 pc away (Bailer-Jones *et al.* 2021).

BI Ceti (BI Cet) is a known FIRST radio star. It was first detected in the radio by Drake, Simon, & Linsky (1986) using the VLA. BI Cet is an RS CVn binary consisting of a G6IV/V star and a G6V star (Kozhevnikova & Alekseev 2015) $62.12^{+0.07}_{-0.1}$ pc away (Bailer-Jones *et al.* 2021).

39 Ceti (39 Cet) is a known FIRST radio star. It was first detected in the radio by Simon, Fekel, & Gibson (1982) using the VLA. It is an RS CVn type binary consisting of a G5III star

and a DA2.8 white dwarf (e.g. Luck 2015) 74.6 ± 0.5 pc away (Bailer-Jones *et al.* 2021).

FK Comae Berenices (FK Com) is a known FIRST radio star. It has been detected in both Stokes I and Stokes V at 144 MHz with LOFAR (Toet *et al.* 2021). FK Com is an FK Com type G star (a single star that was a binary, but merged) $222.8^{+1.4}_{-1.3}$ pc away (Bailer-Jones *et al.* 2021).

BH Canum Venaticorum (BH CVn) is a known FIRST and NVSS radio star and it has also been detected at 144 MHz in both Stokes I and V by LOFAR (Toet *et al.* 2021; Vedantham *et al.* 2022). This source was found by Pritchard *et al.* (2021) in their search for circularly polarised sources with ASKAP. BH CVn is an RS CVn type binary and is 46.8 ± 0.2 pc away (Bailer-Jones *et al.* 2021).

4. Candidate variable stellar radio sources

In Section 2 we described our steps for proper-motion matching. In step 5 we discard the *Gaia* sources and corresponding survey A sources that do not match a survey B source. However, if survey B is equally sensitive or more sensitive than survey A it is interesting to explore the survey A and *Gaia* matches that do not correspond to a survey B source. This is because it means that a radio source was detected in an earlier epoch but was not detected in a later epoch even though the later epoch is from a more sensitive survey. A diagram demonstrating sources that would be considered variables in this way is shown in Figure 5. These sources are likely radio variables, and may indicate that the initial radio detection was from e.g. a stellar flare. Due to the filtering we do to search for proper-motion stars, this is not a complete search for radio variables. We will only find radio variables that match an optical source, which means we will miss those radio variables where the survey A source does not have an optical match. We also only

Table 2. Summary of the position (J2000 reference frame) information for each radio stellar source found using the proper-motion method. ‘F’ stands for FIRST. Survey B indicates the second radio survey used to find the source, either VLASS or RACS-mid. $D_{A,B}$ is the separation in arcseconds between the position of the source in Survey A and the position of the source in Survey B, see Figure 3.

<i>Gaia</i>			FIRST				Survey B							
Name	Position	Epoch	Name	Position	Epoch	$D_{G,F}$	Survey B	Name	Position	Epoch	$T_{F,B}$	$D_{G,B}$	$D_{F,B}$	$D_{G,B}$
PM	15:58:44.97	J2016.0	FIRST	15:58:45.1	J1995.951	0.80''	RACS-mid	ASKAP	15:58:44.9	J2021.009	25.058 yr	2.93''	3.31''	0.62''
J15587	+23:51:17.87		J155845.0	+23:51:19.5				J155844.94	+23:51:17.0					
	+2351E		+235119					+235117.02						
GS Leo	9:30:35.62	J2016.0	FIRST	9:30:35.8	J2000.026	0.06''	VLASS	VLASS1QLCIR	9:30:35.6	J2017.752	17.726 yr	3.55''	3.59''	0.10''
	+10:36:06.04		J093035.8	+10:36:06.3				J093035.59	+10:36:06.1					
			+103606					+103606.1						
							RACS-mid	ASKAP	9:30:35.6	J2021.044	21.018 yr	4.21''	4.33''	0.67''
								J93035.55	+10:36:05.3					
								+103605.31						
sig	16:14:40.51	J2016.0	FIRST	16:14:41.0	J1994.471	0.14''	VLASS	VLASS1QLCIR	7:43:18.6	J2017.762	23.291 yr	6.57''	6.49''	0.21''
CrB A	+33:51:29.62		J161440.9	+33:51:31.6				J161440.48	+28:53:02.2					
			+33					+335129.5						
							RACS-mid	ASKAP	16:14:40.4	J2020.998	26.527 yr	7.48''	8.41''	1.99''
								J161440.40	+33:51:27.2					
								+335127.20						
sig Gem	7:43:18.80	J2016.0	FIRST	7:43:18.6	J1993.328	0.64''	VLASS	VLASS1QLCIR	7:43:18.8	J2019.279	25.951 yr	6.16''	6.39''	0.24''
	+28:52:56.96		J074318.6	+28:53:02.2				J074318.83	+28:52:56.3					
			+285302					+285256.30						
							RACS-mid	ASKAP	7:43:18.8	J2021.011	27.683 yr	6.57''	7.53''	0.73''
								J74318.84	+28:52:55.1					
								+285255.10						
Bl Cet	1:22:50.17	J2016.0	FIRST	1:22:50.3	J1998.774	0.63''	VLASS	VLASS1QLCIR	1:22:50.2	J2017.738	18.964 yr	5.03''	4.62''	0.30''
	+0:42:39.57		J012250.3	+0:42:43.3				J012250.16	+0:42:39.4					
			+004243					+004239.4						
							RACS-mid	ASKAP	1:22:50.1	J2021.029	22.255 yr	5.90''	5.50''	0.42''
								J12250.13	+0:42:38.8					
								+004238.77						
39 Cet	1:16:36.18	J2016.0	FIRST	1:16:36.3	J1998.172	0.49''	VLASS	VLASS1QLCIR	1:16:36.2	J2017.790	19.618 yr	2.33''	2.48''	0.17''
	-2:30:02.35		J011636.2	-2:30:00.7				J011636.16	-2:30:02.3					
			-023000					-023002.2						
							RACS-mid	ASKAP	1:16:36.2	J2020.991	22.819 yr	2.71''	3.49''	1.18''
								J11636.18	-2:30:03.7					
								-023003.74						
FK Com	13:30:46.74	J2016.0	FIRST	13:30:46.8	J1995.942	0.57''	VLASS	VLASS1QLCIR	13:30:46.7	J2017.751	21.809 yr	1.23''	1.57''	0.09''
	+24:13:57.43		J133046.8	+24:13:58.4				J133046.73	+24:13:57.4					
			+241358					+241357.4						
BH CVn	13:34:47.92	J2016.0	FIRST	13:34:47.8	J1994.560	0.10''	VLASS	VLASS1QLCIR	13:34:48.0	J2017.824	23.264 yr	2.00''	2.13''	0.22''
	+37:10:56.54		J133447.7	+37:10:56.7				J133447.95	+37:10:56.5					
			+371056					+371056.5						

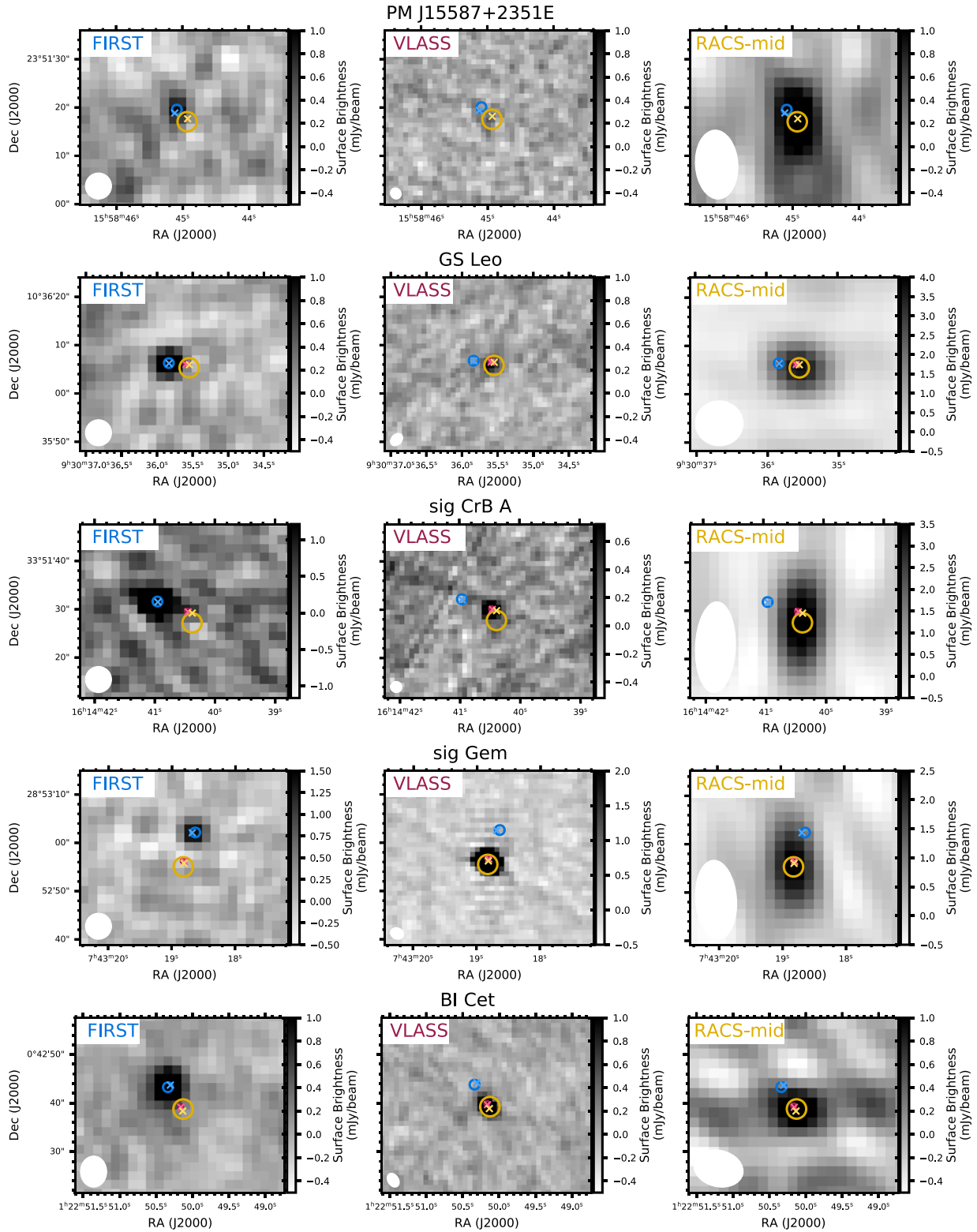


Figure 4. Radio images of the stellar sources found using radio proper-motion. The cross-hairs indicate the *Gaia* DR3 proper-motion corrected position corrected to the epoch of the radio image. The circles indicate the radio position of the source and the radius is the uncertainty on the radio position: FIRST, cyan, 1"; VLASS, magenta, 0.5"; and RACS-mid, yellow, 2". The grey scale is not the same for every panel. PM J15587+2351E is not detected by VLASS. Both FK Com and BH CVn were only found using the proper-motion method with FIRST and VLASS, they were not found using FIRST and RACS-mid as the separation between the FIRST position and the RACS-mid position is $< 3''$. However, both sources are detected by RACS-mid, as we can see in these plots.

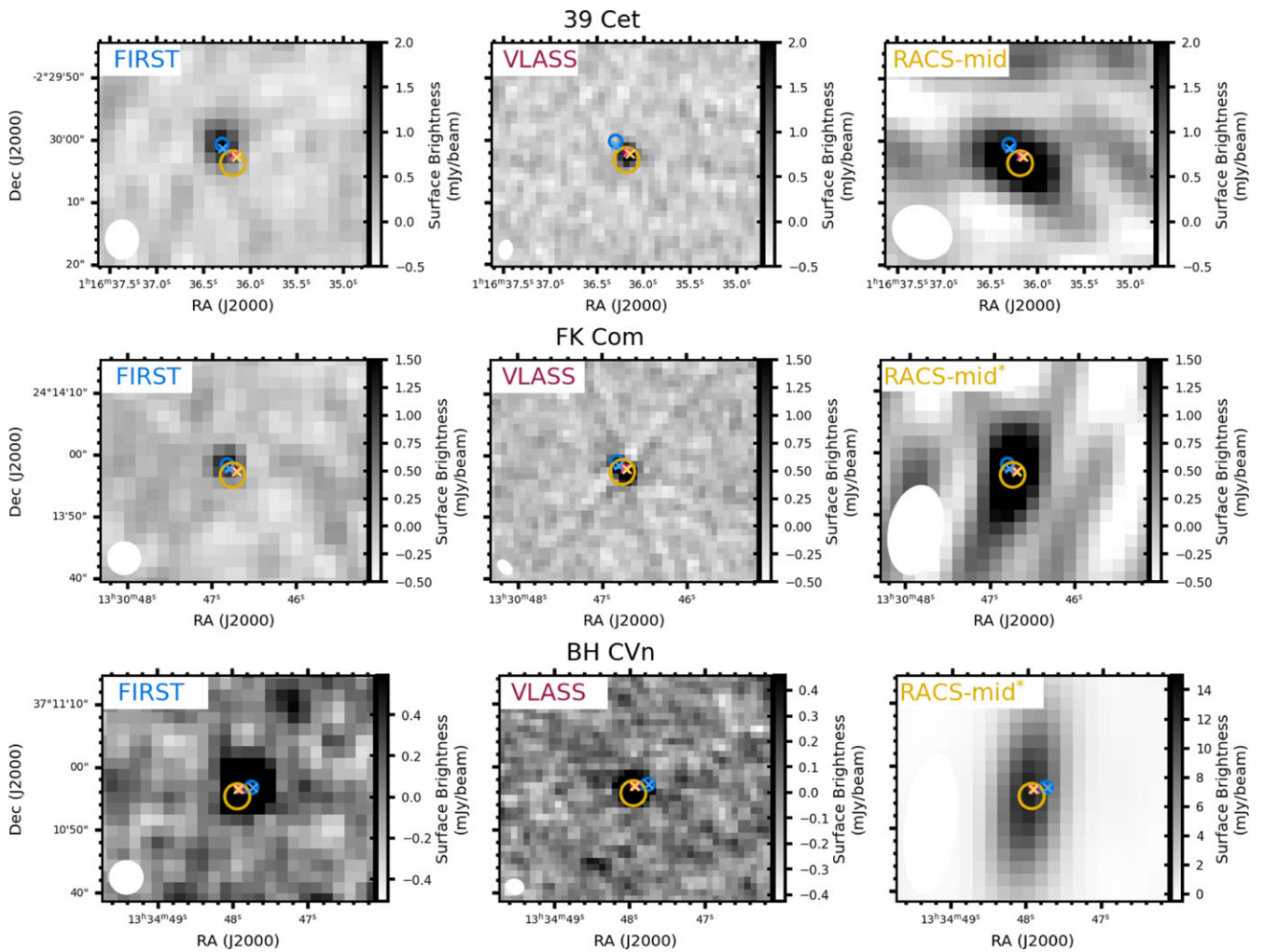


Figure 4. Continued.

match to optical sources with a proper-motion measurement in *Gaia*, further reducing the sample.

The steps we used to find candidate variable stars are as follows:

1. Discard *Gaia* sources that have no measured proper-motion magnitude
2. Discard sources in survey A where $F_{\text{int}}/F_{\text{peak}} \geq 1.5$. Do not do this for survey B.
3. Keep any survey A sources that are separated by $> a'' + b''$ from all survey B sources and keep any survey B sources that are separated by $> a'' + b''$ from all survey A sources
4. Proper-motion correct the *Gaia* source positions to the survey A epoch and cross-match the source positions. The sources are considered a match if the separation is $< a''$. Discard those *Gaia* and survey A sources that do not match.
5. Proper-motion correct the remaining *Gaia* source positions to the survey B epoch and cross-match the source positions. The sources are considered a match if the separation is $< b''$. Discard those *Gaia* and survey B sources that **do** match.

6. Discard *Gaia* sources (and the corresponding FIRST matches) that have a parallax over error < 5 .

We perform these steps with FIRST as survey A and treat each of VLASS, RACS-low and RACS-mid separately as survey B. However, there are sources in common between the different surveys. At this point, we combine the three separate FIRST-VLASS, FIRST-RACS-low, FIRST-RACS-mid catalogues into one catalogue. We are then working with the combined catalogue for the following steps:

7. Discard sources where $D_{\text{FIRST,RACS-mid}} < 3''$
8. Discard sources outside the RACS-mid FoV, i.e. sources with declination $> 45^\circ$
9. Discard sources where $D_{\text{FIRST,VLASS}} < D_{\text{GVLASS,VLASS}}$

In step (2) we do not remove resolved sources from survey B as faint point sources in survey A might be revealed as extended sources in survey B. In step (5) we remove the sources that do have a proper-motion match, as the sources with a proper-motion match are the stars presented in Section 3. In step (6) we use the *Gaia* parallax over error, the parallax value divided by the

Table 3. Flux densities for the radio stellar sources found using proper motion. FK Com and BH CVn were not detected in RACS-mid using the proper-motion method as the RACS-mid position is $<3''$ from the FIRST position. However, we know that these sources are radio stars from FIRST–VLASS proper-motion matching. We have therefore included their RACS-mid flux densities in this table. Some sources are detected in RACS-mid more than once as they fall in the overlap between tiles. The FIRST survey catalogue does not include uncertainties on the peak flux density.

Name	Survey	Freq (MHz)	Epoch	F_{peak} (mJy)
PM J15587+2351E	FIRST	1 400.0	J1995.95	1.3
	RACS-MID	1 367.5	J2021.01	1.6 ± 0.2
GS Leo	FIRST	1 400.0	J2000.03	2.3
	VLASS	3 000.0	J2017.75	1.4 ± 0.1
	RACS-MID	1 367.5	J2021.04	3.9 ± 0.3
sig CrB A	FIRST	1 400.0	J1994.47	5.5
	VLASS	3000.0	J2017.76	3.2 ± 0.2
	RACS-MID	1 367.5	J2021.00	4.3 ± 0.4
sig Gem	FIRST	1 400.0	J1993.33	2.0
	VLASS	3 000.0	J2019.28	54.2 ± 0.1
	RACS-MID	1 367.5	J2021.01	2.6 ± 0.3
Bl Cet	FIRST	1 400.0	J1998.77	2.0
	VLASS	3 000.0	J2017.74	3.4 ± 0.1
	RACS-MID	1 367.5	J2021.03	1.4 ± 0.2
39 Cet	FIRST	1 400.0	J1998.17	2.2
	VLASS	3 000.0	J2017.79	2.7 ± 0.2
	RACS-MID	1 367.5	J2020.99	3.0 ± 0.5
	RACS-MID	1 367.5	J2020.99	2.4 ± 0.3
FK Com	FIRST	1 400.0	J1995.94	1.8
	VLASS	3 000.0	J2017.75	8.0 ± 0.1
	RACS-MID	1 367.5	J2020.99	2.7 ± 0.3
	RACS-MID	1 367.5	J2021.00	2.0 ± 0.3
BH CVn	FIRST	1 400.0	J1994.56	4.0
	VLASS	3 000.0	J2017.82	9.5 ± 0.1
	RACS-MID	1 367.5	J2020.98	13.1 ± 0.8

uncertainty, to reduce the number of extra-galactic sources in our sample. This is because the parallax over error represents the signal to noise of the parallax measurement, and extra-galactic sources typically have lower uncertainty-normalised parallax measurements as they are fainter. We perform steps (1) to (6) on each of VLASS, RACS-low and RACS-mid, with FIRST as survey A. However, RACS-mid (1 367 MHz) is the closest in frequency to FIRST (1 400 MHz), so we find these sources to be the strongest candidates. This is why we include step (7). We find that there are some sources where the VLASS–FIRST separation ($D_{\text{FIRST,VLASS}}$) is less than the VLASS–proper-motion corrected *Gaia* position separation ($D_{\text{GVLASS,VLASS}}$). This means that the optical source is less likely to be responsible for the radio emission. We remove such sources in step (9).

After performing steps (1) to (5) we are left with FIRST sources that are matched to *Gaia* proper-motion sources, but do not have a match in one of VLASS, RACS-low or RACS-mid either at the FIRST position or at the *Gaia* proper-motion corrected position. At this point, we find 4 638, 4 748, and 2 768 candidate variable radio sources when we compare FIRST to VLASS, RACS-low, and

RACS-mid respectively.^c After these steps, many of these sources are likely to still be extra-galactic sources. We do not investigate most of these sources further.

After applying the parallax cut (step (6)), we are left with 76, 88, and 115 candidate variable radio stellar sources when we compare FIRST to VLASS, RACS-low, and RACS-mid respectively. It is at this point that we combine the individual VLASS, RACS-low, and RACS-mid candidates into one catalogue of 156 total unique candidate variable radio stellar sources. After performing steps (7) to (9) we have 62 remaining candidate variable radio stellar sources. Finally, we manually check the FIRST and VLASS images and remove any sources that are extended or appear to be artefacts. This eliminates 8 sources, leaving 54 sources in our final set of candidate variable radio stellar sources. We present the *Gaia* positions and the separations between the FIRST position and nearest VLASS, RACS-low and RACS-mid sources in Table 4.

We performed a simulation of steps 1 to 6 to determine how likely it is that the 54 candidate variable radio stars are chance coincidence between the radio source and an optical source. We did this using FIRST, *Gaia* and RACS-mid. We took the positions of the FIRST sources and randomised their Right Ascension and Declination. We offset each source by taking the square root of a number drawn from a random uniform distribution between shift^2 and $(\text{shift}+\text{radius})^2$ where $\text{shift}=2''$ and $\text{radius}=15''$. This offset was in a direction chosen by selecting an angle between 0 and 360 from a random uniform distribution. We chose a minimum shift of $2''$ as our match radius is $1''$ and we did not want real matches in our random matches. We similarly randomised the positions of the RACS-mid sources using a $\text{shift}=4''$ and $\text{radius}=15''$. We also needed to account for proper-motion. We selected a FIRST epoch by drawing from a random uniform distribution with a minimum and maximum matching the first and last FIRST epochs. We did the same to select a RACS-mid epoch. We then used the randomised FIRST and RACS-mid positions and epochs to perform steps 1 to 6. We performed this 50 000 times and recorded the number of resultant candidate variable stars per iteration. This resulted in a Poisson distribution with $\lambda = 3.2$, where λ is the expectation value and variance of the distribution. This means that it is likely that between 1 and 5 of the 54 matches are chance coincidence.

Nine of the sources, marked by numbers in Table 5 have previously been identified as radio stars. We searched the literature and archives to further investigate the candidate variable radio stellar sources. We searched each survey/catalogue within $1''$ of the FIRST position of each source. Many of the sources have been classified as optical counterparts to radio sources in the past, the results of the search are shown in Table 5. In the table and in the descriptions here we have used ‘stellar’ and ‘star’ as in the original references. ‘Stellar’ is used to mean a source with an unresolved or point-like point spread function (PSF), while a ‘star’ is ‘a self-luminous gaseous celestial body’ (Ahumada *et al.* 2020).

Becker *et al.* (2001) and McMahon *et al.* (2002) matched FIRST sources to the Cambridge Automated Plate Measuring Machine (APM) scans of the POSS I plates. Becker *et al.* (2001) used a match radius of $1'.2$ while McMahon *et al.* (2002) used a match radius of $5''$ between FIRST and APM sources. In both of these surveys a source is classified as ‘stellar’ if the optical source had an unresolved or ‘point-like’ PSF in the relevant optical

^cThe variable source candidate catalogue at this point is available in the supplementary material.

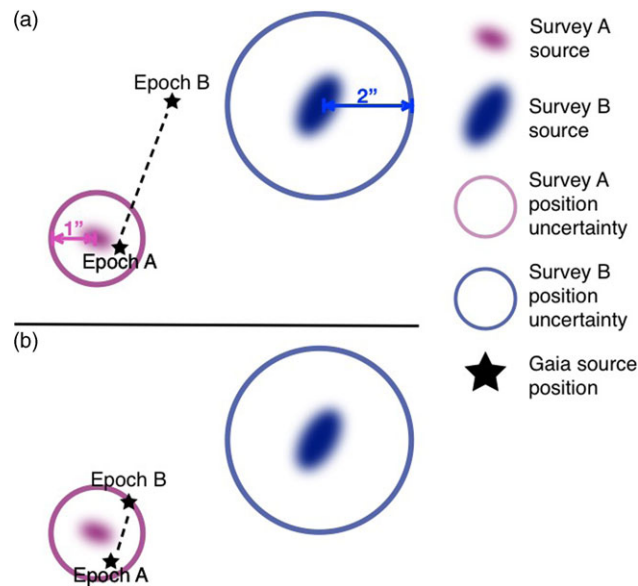


Figure 5. Diagram illustrating two *Gaia* sources which would be considered candidate radio variable stellar sources. In both cases (a) and (b) the optical source does match a radio source in survey A but does not match a source in survey B.

survey. McMahon et al. (2002) performed extensive exploration of the chance coincidence and completeness of the matching and estimated that 98% of APM sources within $1''$ of a FIRST source were physically associated.

45 of the sources were classed as matches to Sloan Digital Sky Survey (SDSS; Abazajian et al. 2009) ‘stellar’ sources by Helfand, White, & Becker (2015). In the SDSS catalogue stellar sources are mostly quasars and AGN with a smaller fraction of radio stars. They matched FIRST and SDSS using a $4''.8$ match radius, they found that 19% of FIRST-SDSS matches at a radius of $4''.8$ are false/chance.

Eight of the sources were classed as candidate radio stars by Kimball et al. (2009). They matched FIRST and SDSS using a match radius of $1''$. They also filtered the SDSS optical sources such that $r \leq 20.5$ mag and the FIRST radio sources such that $S_{20} \geq 1.25$ mJy (where S_{20} is the FIRST flux density). Using these criteria they found that 98% of their matches were physically associated. After matching, they filtered out quasars from the sample using SDSS spectra and literature investigations of the sources. They then visually inspected the radio sources and removed any resolved or complex morphology sources. However, they concluded that most if not all of their candidate stellar radio sources were actually chance alignments between the radio and optical.

26 of the sources were classed as stars in the Million Optical–Radio/X-ray (MORX; Fleisch & Hardcastle 2004; Fleisch 2016) Associations Catalogue. They used an algorithm described in Fleisch & Hardcastle (2004) to calculate the likelihood of each match. The confidence of the match is included in the catalogue.

42 of the sources match within $1''$ of at least one SDSS Data Release 16 (SDSS DR16; Ahumada et al. 2020) source. SDSS also classes their sources as either a galaxy or a star. 28 of the sources have only stars within $1''$ of the FIRST position, while 14 have at least one source classed as a galaxy or unknown within $1''$ of the FIRST position. The matches to these catalogues for each of our 54 candidate variable radio stellar sources are shown in Table 5.

The distances to these sources range from ~ 30 pc (HD 77407) to $\sim 2\,300$ pc (Gaia DR3 6910163884580689280).

We used the literature search to investigate some sources in more detail. In particular, we checked those sources that were classed as galaxies by Helfand et al. (2015) and those sources where there is a galaxy within $1''$ as determined by Ahumada et al. (2020). Some of these sources (BD+09 4984B, TYC 2503-1270-1, V* FF Aqr, V* IN Leo, V* V436 Ser, HD 77407, V* AZ Psc, V* MS Ser) are well-known stars that were mis-classified as galaxies as they are extremely bright optical sources. Two sources (Gaia DR3 2377310715263856512 and 2MASS J07415981+2331589) are unlikely to be radio stars.

Gaia DR3 2377310715263856512 and 2MASS J07415981+2331589 are less than $2''$ from faint optical sources that do not have parallax or proper-motion measurements. These nearby optical sources may be galaxies and as such we find it more likely that the radio emission is associated with these galaxies. We conclude that we have found nine previously known variable radio stars and 43 candidate variable radio stars; where 5 candidates are likely to be chance coincidence.

5. Discussion

We have found eight radio stars using their proper-motion, two of which (PM J15587+2351E and GS Leo) have not previously been identified as radio stars. We have also found 43 candidate variable radio stellar sources and nine known radio stars.

The set of proper-motion radio stars is likely volume limited. This is because the further the star is from Earth, the further the star needs to travel to achieve a high proper-motion (all of the following proper-motion calculations are in two dimensions). In the set of RACS-mid detected stars, sig Gem travels the furthest: 0.001 pc. The smallest $D_{\text{GIRST, RM}}$ value for RACS-mid detected stars is 39 Cet: $2.71''$. The distance at which 0.001 pc $\approx 2.71''$ is ~ 90 pc. This provides an approximate maximum distance that we have

Table 4. Details of the 54 candidate variable radio stellar sources. We include both the optical/Simbad name (or *Gaia* DR3 designation where a Simbad name is not available) and the FIRST name for each source. In the columns where we give the separations between source positions, 'F' is for FIRST, 'RL' is for RACS-low, 'RM' is for RACS-mid and 'V' is for VLASS. The FIRST survey catalogue does not include uncertainties on the peak flux density and the typical RMS noise values for FIRST, RACS-low, RACS-mid and VLASS are shown in Table 1. A machine-readable version of this table is available in the supplementary material.

Name	Gaia J2016	FIRST			VLASS			RACS-low			RACS-mid			
		Epoch	Gaia sep (")	Flux density (mJy)	Epoch	Gaia sep (")	FIRST sep (")	Epoch	Gaia sep (")	FIRST sep (")	Epoch	Gaia sep (")	FIRST sep (")	
2MASS J07500030+3458579	FIRST J075000.2+345858	7:50:00.3 +34:58:57.7	J1994.5	0.78	1.82	J2019.4	0.69	186.33				J2021.0	0.73	3.41
2MASS J08293480+0858099	FIRST J082934.8+085809	8:29:34.8 +8:58:10.2	J2000.1	0.65	1.41	J2017.8	0.52	68.03	J2019.3	0.57	69.59	J2021.0	0.62	68.04
2MASS J09244488+0019097	FIRST J092444.8+001908	9:24:44.9 +0:19:09.7	J1998.6	0.91	1.98	J2018.0	0.08	338.12	J2019.3	0.08	178.17	J2021.0	0.09	178.22
2MASS J09420757+0334344	FIRST J094207.5+033434	9:42:07.6 +3:34:34.4	J1998.5	0.47	1.15	J2018.0	0.10	14.30	J2020.3	0.11	9.46	J2021.0	0.12	13.28
2MASS J09582770+2847572	FIRST J095827.7+284757	9:58:27.8 +28:47:57.2	J1993.3	0.87	1.06	J2019.3	0.95	324.92	J2020.3	0.99	94.92	J2021.0	1.01	79.33
2MASS J10014486+2756455	FIRST J100144.7+275645	10:01:44.8 +27:56:45.2	J1995.8	0.93	1.03	J2019.3	0.81	98.80	J2020.3	0.84	98.26	J2021.0	0.86	98.89
2MASS J14333139+3417472	FIRST J143331.5+341747	14:33:31.3 +34:17:46.8	J1994.5	0.87	1.23	J2017.9	2.28	249.63				J2021.0	2.58	6.88
2MASS J15085996+2714307	FIRST J150859.9+271430	15:09:00.0 +27:14:30.5	J1995.9	0.57	1.06	J2017.8	0.36	397.11	J2020.3	0.40	31.03	J2021.0	0.41	181.18
2MASS J15215160+4246246	FIRST J152151.6+424624	15:21:51.6 +42:46:24.5	J1996.0	0.24	2.4	J2019.2	0.20	0.61				J2021.0	0.21	3.74
2MASS J16234398+1302124	FIRST J162343.9+130211	16:23:44.0 +13:02:11.9	J2000.0	0.95	1.08	J2019.3	0.65	188.54	J2019.3	0.65	188.55	J2021.1	0.71	60.35
2MASS J20485716-0053473	FIRST J204857.2-005348	20:48:57.3 -0:53:48.5	J2011.3	0.15	1.94	J2018.0	0.67	221.63	J2019.3	0.80	221.93	J2021.0	0.97	220.96
BD+09 4984B	FIRST J220611.8+100528	22:06:11.8 +10:05:28.6	J2011.2	0.57	2.22	J2017.7	0.04	271.77	J2019.3	0.05	367.67	J2021.6	0.07	271.80
BD-08 6022	FIRST J230553.0-074548	23:05:53.0 -7:45:48.9	J2011.3	0.18	3.74	J2017.9	0.23	74.80	J2019.3	0.27	52.94	J2021.0	0.33	53.73
LP 521-15	FIRST J224656.1+143715	22:46:56.3 +14:37:15.3	J2011.3	0.80	1.67	J2017.8	2.23	377.34	J2020.5	3.17	376.09	J2021.0	3.35	377.14
Gaia DR3 1158730503710098688	FIRST J144724.8+043700	14:47:24.9 +4:37:00.4	J2000.7	0.57	1.06	J2019.2	0.05	143.84	J2019.3	0.05	145.28	J2021.1	0.05	145.65
Gaia DR3 1360691101602998784	FIRST J172747.2+440031	17:27:47.2 +44:00:31.8	J1995.6	0.59	1.38	J2019.3	0.14	55.28				J2021.0	0.15	50.71
Gaia DR3 1732181789609582208	FIRST J211059.8+042632	21:11:00.0 +4:26:33.0	J2009.2	0.77	1.55	J2017.8	0.06	161.75	J2019.3	0.07	160.18	J2021.1	0.08	161.23
Gaia DR3 2377310715263856512	FIRST J003921.0-111037	0:39:21.1 -11:10:37.4	J1997.4	0.61	1.08	J2017.9	0.25	120.27	J2020.2	0.28	42.83	J2021.0	0.29	37.07
Gaia DR3 2467183490048356864	FIRST J014456.9-071309	1:44:56.9 -7:13:09.1	J2009.3	0.98	1.01	J2017.9	0.38	49.55	J2019.3	0.44	49.79	J2021.0	0.51	49.96
Gaia DR3 2490713524213973248	FIRST J020618.5-055910	2:06:18.5 -5:59:10.3	J1997.4	0.61	1.05	J2017.9	0.23	575.65	J2020.2	0.25	131.36	J2021.0	0.26	131.28
Gaia DR3 2633166727449471360	FIRST J233453.9-043809	23:34:53.9 -4:38:09.3	J2011.2	0.31	2.67	J2017.9	0.06	88.05	J2019.3	0.08	89.06	J2021.0	0.09	58.60
Gaia DR3 2715431259726742784	FIRST J230214.6+104205	23:02:14.7 +10:42:05.9	J2011.3	0.68	1.69	J2017.8	0.33	99.21	J2019.3	0.40	98.71	J2021.6	0.52	98.74
Gaia DR3 2776753256590751104	FIRST J005348.1+124519	0:53:48.1 +12:45:18.9	J2011.2	0.88	1.25	J2017.8	0.16	282.10	J2019.3	0.20	292.79	J2021.0	0.24	114.92
Gaia DR3 3147019745776728448	FIRST J075700.2+091955	7:57:00.2 +9:19:55.0	J2000.1	0.69	1.25	J2017.9	0.06	2.03	J2019.3	0.07	3.81	J2021.0	0.07	165.97
Gaia DR3 3592258045911461376	FIRST J075700.2+091955	11:42:12.2 -7:53:59.4	J2001.4	0.12	1.0	J2019.4	0.32	173.30	J2019.3	0.32	175.22	J2021.0	0.35	174.17
Gaia DR3 6910163884580689280	FIRST J205141.4-063340	20:51:41.4 -6:33:40.6	J2011.3	0.41	1.03	J2019.3	0.07	86.33	J2019.3	0.07	85.85	J2021.0	0.08	85.17
SDSS J161007.07+394132.8	FIRST J161007.0+394132	16:10:07.1 +39:41:32.7	J1994.6	0.48	1.13	J2017.8	0.17	143.76				J2021.0	0.19	231.72
StKM 1-1155	FIRST J142555.9+141210	14:25:55.9 +14:12:09.6	J2000.0	0.51	1.73	J2019.3	1.29	502.20	J2020.3	1.36	2.16	J2021.1	1.41	453.37
TYC 2503-1270-1	FIRST J100502.4+301824	10:05:02.4 +30:18:24.0	J1993.3	0.53	1.35	J2019.3	0.99	315.37				J2021.0	1.05	3.91

Table 4. Continued.

Name	Gaia J2016	FIRST			VLASS			RACS-low			RACS-mid		
		Epoch	Gaia sep (")	Flux density (mJy)	Epoch	Gaia sep (")	FIRST sep (")	Epoch	Gaia sep (")	FIRST sep (")	Epoch	Gaia sep (")	FIRST sep (")
UCAC4 431–063012 FIRST J155042.6–035846	15:50:42.6 – 3:58:46.6	J1999.0	0.96	1.68	J2019.3	0.52	170.52	J2019.3	0.52	169.55	J2022.4	0.60	170.01
V* FF Aqr FIRST J220036.4–024427	22:00:36.5 – 2:44:27.0	J2011.2	0.26	2.39	J2017.7	0.22	0.53	J2019.3	0.27	235.86	J2021.0	0.32	113.26
V* IN Leo FIRST J103959.0+132722	10:39:59.0 + 13:27:21.6	J2000.0	0.28	1.95	J2018.0	0.47	0.60	J2019.3	0.50	102.61	J2021.0	0.55	102.02
V* V436 Ser FIRST J152346.1–004424	15:23:46.1 – 0:44:24.8	J1998.6	0.50	2.63	J2019.3	0.28	209.57	J2019.3	0.28	209.95	J2022.4	0.33	209.51
Wolf 424 A FIRST J123317.3+090115	12:33:15.5 + 9:01:19.5	J2000.1	0.23	1.41	J2019.3	34.78	200.94	J2020.3	36.54	282.36	J2021.0	37.80	276.49
Wolf 424 B FIRST J123317.3+090115	12:33:15.5 + 9:01:18.6	J2000.1	0.80	1.41	J2019.3	33.12	200.94	J2020.3	34.79	282.36	J2021.0	36.00	276.49
[UBW2009] 21 FIRST J090624.3+001537	9:06:24.4 + 0:15:38.0	J1998.6	0.97	1.04	J2017.7	0.24	265.78	J2019.3	0.26	265.39	J2021.0	0.29	265.48
Gaia DR3 1157257742244515584 FIRST J150822.1+061436	15:08:22.2 + 6:14:37.5	J2000.1	0.73	1.02	J2019.2	0.08	257.55	J2020.3	0.08	258.67	J2021.1	0.08	123.80
Gaia DR3 1305574679646964352 FIRST J162716.0+275658	16:27:16.0 + 27:56:57.8	J1995.8	1.00	1.19	J2017.9	0.22	15.74	J2020.3	0.24	16.01	J2021.0	0.25	14.46
2MASS J03065628+0044316 FIRST J030656.2+004431	3:06:56.3 + 0:44:31.6	J1997.4	0.52	0.97	J2017.9	0.04	279.99	J2019.3	0.04	281.11	J2021.0	0.05	280.04
2MASS J07415981+2331589 FIRST J074159.8+233158	7:41:59.8 + 23:31:58.9	J1996.0	0.81	1.29	J2019.3	0.08	183.03	J2019.3	0.08	192.39	J2021.0	0.08	192.81
2MASS J16115068+4344126 FIRST J161150.6+434412	16:11:50.7 + 43:44:12.7	J1994.6	0.23	1.2	J2019.3	0.26	61.03				J2021.0	0.28	46.49
2MASS J16235772+2350113 FIRST J162357.7+235010	16:23:57.7 + 23:50:11.2	J1996.0	0.63	1.88	J2017.7	0.23	120.75	J2020.3	0.26	126.80	J2021.0	0.27	110.83
FBQS J0748+3709 FIRST J074809.7+370926	7:48:09.8 + 37:09:26.1	J1994.6	0.61	1.05	J2019.3	0.10	96.21				J2021.0	0.11	98.10
FBQS J0754+3937 FIRST J075413.7+393720	7:54:13.8 + 39:37:20.0	J1994.6	0.67	1.25	J2019.3	0.11	214.60				J2021.0	0.12	6.61
FBQS J1216+3020 FIRST J121624.2+302042	12:16:24.2 + 30:20:42.3	J1993.3	0.60	1.06	J2017.9	0.45	37.68				J2021.0	0.50	38.52
FBQS J1421+3319 FIRST J142142.1+331935	14:21:42.1 + 33:19:35.7	J1995.0	0.99	1.12	J2017.9	0.44	215.94				J2021.0	0.50	4.29
FBQS J1704+2931 FIRST J170411.6+293153	17:04:11.6 + 29:31:52.9	J1994.7	0.61	1.13	J2017.9	0.24	168.86				J2021.0	0.27	180.45
FBQS J1707+3802 FIRST J170718.5+380204	17:07:18.5 + 38:02:04.4	J1994.6	0.52	1.04	J2017.9	0.16	65.35				J2021.0	0.18	63.79
FIRST J093148.2+394833	9:31:48.3 + 39:48:33.2	J1994.6	0.15	1.23	J2019.3	0.10	244.40				J2021.0	0.11	6.76
HD 77407 FIRST J090327.0+375029	9:03:27.0 + 37:50:26.6	J1994.6	0.96	1.67	J2019.3	4.35	29.74				J2021.0	4.64	8.15
PM J11240+3808 FIRST J112404.3+380810	11:24:04.5 + 38:08:10.7	J1994.6	0.34	1.14	J2019.3	3.02	371.00				J2021.0	3.22	287.66
V* AZ Psc FIRST J225852.9–001857	22:58:53.0 – 0:18:57.2	J1999.2	0.30	2.28	J2018.0	1.08	132.27	J2019.3	1.15	130.95	J2021.0	1.25	132.10
V* FP Cnc B FIRST J080855.4+324906	8:08:55.4 + 32:49:01.4	J1994.6	0.26	2.47	J2019.3	5.30	390.49				J2021.0	5.65	261.38
V* MS Ser FIRST J155844.0+253411	15:58:43.9 + 25:34:08.5	J1995.9	0.45	2.28	J2017.9	3.12	315.73	J2020.3	3.46	84.38	J2021.0	3.56	5.92

Table 5. Literature classifications for the candidate variable radio star sources identified using FIRST and RACS-mid. We searched the FIRST position of each source with a 1'' radius in each survey. 'Class' indicates the classification of the source by that survey. The classes from Flesch (2016) are 'S' for star, 'R' for radio, and 'X' for X-ray. Becker et al. (2001), McMahon et al. (2002) and Helfand et al. (2015) use 'stellar' to indicate that the PSF of the optical source is unresolved/point-like, which may include quasars/AGNs as well as stars. "Radio conf" indicates the confidence that the optical-radio match is physical. The separations are the separations between the radio source and the optical counterpart identified. The last three columns indicate whether there is a source classed as a galaxy, star or unknown by SDSS DR16 ('Y' for yes and 'N' for no; Ahumada et al. 2020). Sources marked with a †† were explored further as the literature search showed possible galaxy identification.

Name	McMahon et al. (2002)		Becker et al. (2001)		Helfand et al. (2015)		Kimball et al. (2009)		Flesch (2016)			Ahumada et al. (2020)		
	Sep (")	class	Sep (")	class	Sep (")	class	Sep (")	stellar class	class	radio conf	(")	galaxy within 1''	star within 1''	unknown within 1''
2MASS J07500030+3458579	0.9	stellar			0.92	stellar	0.85	M1	SR	97.8	0	N	Y	N
2MASS J08293480+0858099					0.79	stellar			SR	97.3	0	N	Y	N
2MASS J09244488+0019097					0.94	stellar	0.9	K7				N	Y	N
2MASS J09420757+0334344††					0.37	galaxy			SR	99.0	1	Y	N	N
2MASS J09582770+2847572	2.3	stellar			0.5	stellar	0.44	M3				N	Y	N
2MASS J10014486+2756455	2.1	stellar			0.66	stellar	0.65	M2	SR	89.1	1	N	Y	N
2MASS J14333139+3417472 ¹	4.1	stellar			1.5	stellar								
2MASS J15085996+2714307††	0.43	stellar			0.62	stellar			SR	97.3	0	Y	Y	N
2MASS J15215160+4246246	1.3	noise			0.22	stellar	0.21	M1	SR	98.4	1	N	Y	N
2MASS J16234398+1302124					0.91	stellar			SR	97.2	0	N	Y	Y
2MASS J20485716-0053473					0.57	stellar						N	Y	N
BD+09 4984B††									RX	99.0	0	Y	N	N
BD-08 6022					0.11	stellar			SRX	97.8	0	N	Y	N
LP 521-15					2.8	stellar								
Gaia DR3 1158730503710098688					0.59	stellar						N	Y	N
Gaia DR3 1360691101602998784	0.72	stellar			0.58	stellar			R	99.2	0	N	Y	N
Gaia DR3 1732181789609582208					0.78	stellar						N	Y	Y
Gaia DR3 2377310715263856512					0.57	stellar						Y	Y	N
Gaia DR3 2467183490048356864					0.85	stellar						N	Y	N
Gaia DR3 2490713524213973248					0.51	stellar						N	Y	N
Gaia DR3 2633166727449471360					0.32	stellar						N	Y	Y
Gaia DR3 2715431259726742784					0.62	stellar			R	92.6	1	N	Y	N
Gaia DR3 2776753256590751104					0.78	stellar						N	Y	N
Gaia DR3 3147019745776728448					0.69	stellar			SR	72.0	1	N	Y	N
Gaia DR3 3592258045911461376														
Gaia DR3 6910163884580689280					0.39	stellar			SR	71.1	1	N	Y	N
SDSS J161007.07+394132.8	0.5	stellar			0.47	stellar			SR	98.2	0	N	Y	N
StKM 1-1155					0.34	stellar			SRX	98.7	0	N	Y	N
TYC 2503-1270-1††	4.3	blended			0.36	stellar			SR	92.0	2	Y	Y	N
UCAC4 431-063012														
V* FF Aqr ^{‡,2}					0.54	galaxy			SRX	92.2	1	Y	Y	N
V* IN Leo††					0.47	galaxy			SRX	98.5	0	Y	Y	N
V* V436 Ser††					0.61	stellar			SRX	97.8	0	Y	Y	N
Wolf 424 A ³					6.0	stellar			R	98.7	0			
Wolf 424 B ³					6.0	stellar			R	98.7	0			
[UBW2009] 21					0.98	stellar						N	Y	N
Gaia DR3 1157257742244515584					0.69	stellar	0.71	G6	SR	80.2	1	N	Y	N
Gaia DR3 1305574679646964352	0.49	non-stellar			1.1	stellar								
2MASS J03065628+0044316 ⁴					0.48	stellar			SR	82.3	2	N	Y	Y
2MASS J07415981+2331589††	0.89	stellar	0.82	stellar	0.79	stellar			SR	86.1	1	Y	Y	N
2MASS J16115068+4344126	0.99	stellar			0.17	stellar			SR	79.2	1	N	Y	N

Table 5. Continued.

Name	McMahon et al. (2002)		Becker et al. (2001)		Helfand et al. (2015)		Kimball et al. (2009)		Flesch (2016)			Ahumada et al. (2020)		
	Sep (")	class	Sep (")	class	Sep (")	class	Sep (")	stellar class	radio class	conf	(")	galaxy within 1"	star within 1"	unknown within 1"
2MASS J16235772+2350113	1.3	noise			0.55	stellar	0.57	M3	SR	89.7	1	N	Y	N
FBQS J0748+3709	0.59	stellar	0.52	stellar	0.68	stellar						N	Y	N
FBQS J0754+3937	0.88	stellar	0.33	stellar	0.62	stellar	0.58	F8	SR	98.2	1	N	Y	N
FBQS J1216+3020	1.3	non-stellar			0.39	stellar			R	99.1	0	N	Y	N
FBQS J1421+3319	0.72	stellar	0.51	stellar	1.0	stellar								
FBQS J1704+2931	0.43	stellar	0.43	stellar	0.56	stellar			SR	75.4	1	N	Y	N
FBQS J1707+3802	0.23	stellar	0.23	stellar	0.57	stellar			SR	82.1	1	N	Y	N
FIRST J093148.2+394833	0.25	stellar			0.11	stellar			SR	98.6	0	N	Y	N
HD 77407 ^{4,5}	12	non-stellar			2.5	galaxy								
PM J11240+3808	4.6	stellar			1.2	stellar								
V* AZ Psc ^{4,5}					0.14	galaxy			SRX	57.6	1	Y	N	N
V* FP Cnc B ⁵	18	stellar			1.7	stellar								
V* MS Ser ^{4,5}	9.1	non-stellar			2.3	galaxy								

⁽¹⁾ identified as a radio star using circular polarisation by Callingham et al. (2021a).
⁽²⁾ identified as a radio star by Morris & Mutel (1988).
⁽³⁾ identified as a radio flaring star by Spangler, Shawhan, & Rankin (1974).
⁽⁴⁾ identified as a radio star by Hewett, Foltz, & Chaffee (2001).
⁽⁵⁾ identified as a radio star by Helfand et al. (1999).

Table 6. Time baselines required when performing proper-motion searches between current and future radio sky surveys. t_{\min} is the time it would take to use the proper-motion method to find sig CrB A, the source presented in Section 3 with the highest proper-motion. t_{\max} is the time it would take to use the proper-motion method to find FK Com, the source presented in Section 3 with the lowest proper-motion. MeerKAT has a similar astrometric precision to FIRST, $\sim 1''$, so we have only included FIRST in the table. SKA 0.77 is SKA-low at 770 MHz, SKA 1.4 is SKA-mid at 1.4 GHz, and SKA 6.7 in SKA-mid at 6.7 GHz (Braun et al. 2019).

	FIRST (1")		RACS (2")		VLASS (0.5")		LOTSS (0.2")		SKA 0.77 (0.7")		SKA 1.4 (0.4")		SKA 6.7 (0.08")	
	t_{\min}	t_{\max}	t_{\min}	t_{\max}	t_{\min}	t_{\max}	t_{\min}	t_{\max}	t_{\min}	t_{\max}	t_{\min}	t_{\max}	t_{\min}	t_{\max}
FIRST (1.0")	7.1 yr	35.3 yr	10.6 yr	53.0 yr	5.3 yr	26.5 yr	4.3 yr	21.2 yr	6.0 yr	30.0 yr	5.0 yr	24.7 yr	3.8 yr	19.1 yr
RACS (2.0")	10.6 yr	53.0 yr	14.2 yr	70.7 yr	8.9 yr	44.2 yr	7.8 yr	38.9 yr	9.6 yr	47.7 yr	8.5 yr	42.4 yr	7.4 yr	36.7 yr
VLASS (0.5")	5.3 yr	26.5 yr	8.9 yr	44.2 yr	3.5 yr	17.7 yr	2.5 yr	12.4 yr	4.3 yr	21.2 yr	3.2 yr	15.9 yr	2.1 yr	10.2 yr
LOTSS (0.2")	4.3 yr	21.2 yr	7.8 yr	38.9 yr	2.5 yr	12.4 yr	1.4 yr	7.1 yr	3.2 yr	15.9 yr	2.1 yr	10.6 yr	1.0 yr	4.9 yr
SKA 0.77 (0.7")	6.0 yr	30.0 yr	9.6 yr	47.7 yr	4.3 yr	21.2 yr	3.2 yr	15.9 yr	5.0 yr	24.7 yr	3.9 yr	19.4 yr	2.8 yr	13.8 yr
SKA 1.4 (0.4")	5.0 yr	24.7 yr	8.5 yr	42.4 yr	3.2 yr	15.9 yr	2.1 yr	10.6 yr	3.9 yr	19.4 yr	2.8 yr	14.1 yr	1.7 yr	8.5 yr
SKA 6.7 (0.08")	3.8 yr	19.1 yr	7.4 yr	36.7 yr	2.1 yr	10.2 yr	1.0 yr	4.9 yr	2.8 yr	13.8 yr	1.7 yr	8.5 yr	0.6 yr	2.8 yr

probed by searching for FIRST–RACS–mid proper-motion radio stars. In the set of VLASS detected stars, BI Cet travels the furthest: 0.002 pc, while the smallest $D_{\text{FIRST, RM}}$ value for VLASS detected stars is FK Com: 1.23". The distance at which $0.002 \text{ pc} \approx 1.23''$ is ~ 250 pc. This provides an approximate maximum distance that we have probed by searching for FIRST–VLASS proper-motion radio stars. This means that we can increase the volume we are probing by increasing the time baseline between radio surveys, or decreasing the position uncertainties of the radio surveys, or both. Sensitivity also plays an important role in the volume we can probe to. Pritchard et al. (2021) detected stellar radio sources out to a distance of 150 pc using RACS-low, the RS CVn-like system MKT J170456.2-482100 detected by MeerKAT in ten minute images is 550 pc away (Driessen et al. 2020), and in the set of 8 stellar sources

presented here, FK Com is detected by FIRST, VLASS and RACS-mid at ~ 220 pc. New instruments such as the SKA will be even more sensitive, and therefore will be able to detect stellar sources beyond 250 pc.

To find stars using the proper-motion method we require stars that either have persistent radio emission or are serendipitously flaring in both radio epochs, as well as reasonably high proper-motion. This means that we do not know the expected number of stars that could be detected using the various current and future radio surveys. However, we can use the eight radio stars we have detected with this method to determine the time baseline required for various radio surveys to detect those stars. Of the eight stars we found, FK Com has the lowest proper-motion ($56.615 \text{ mas yr}^{-1}$) and sig CrB A has the highest proper-motion

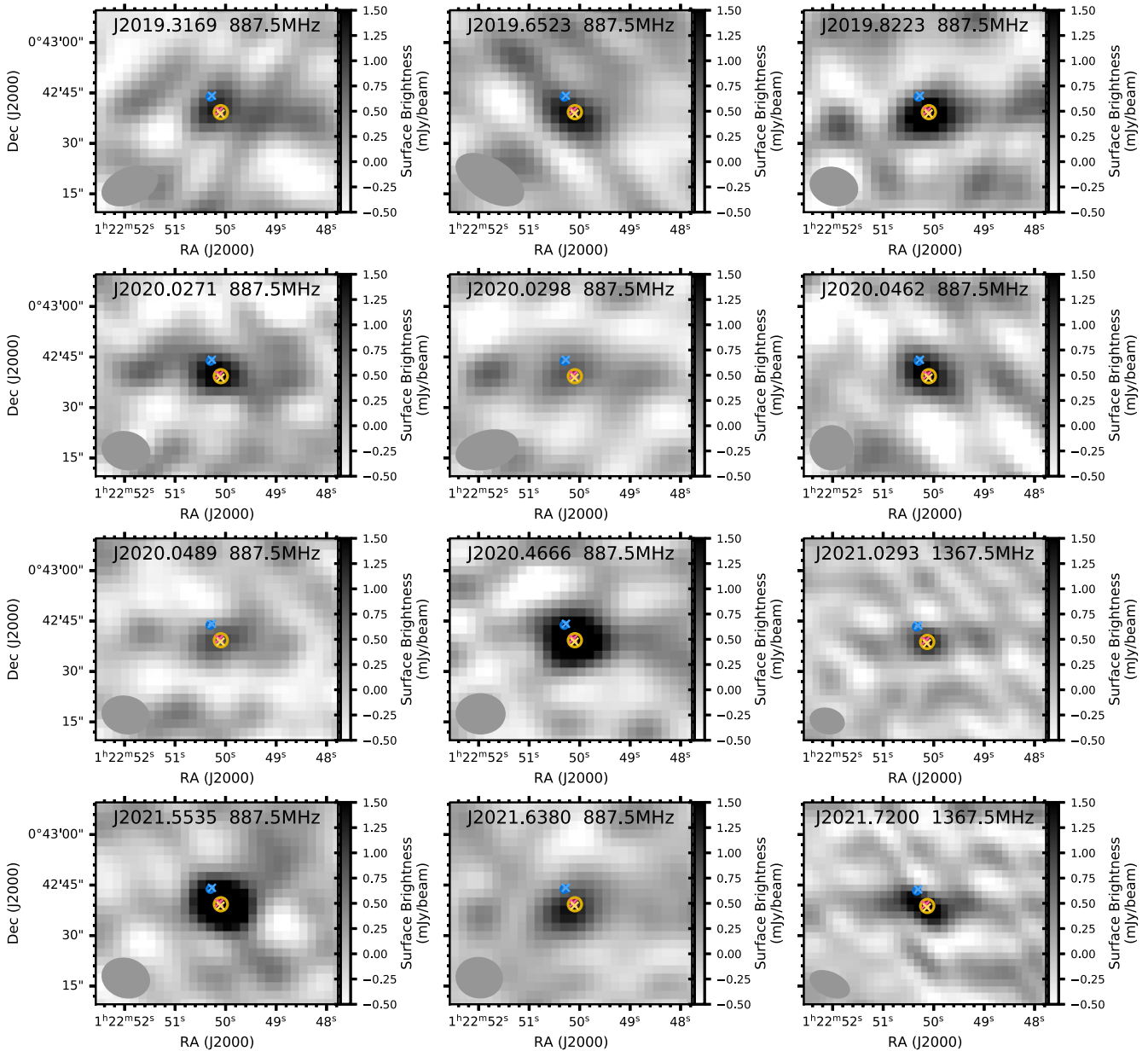


Figure 6. ASKAP images of BI Cet. These images are from the available observations of BI Cet in CASDA, including RACS-low and VAST observations. The epochs and frequencies of the observations are shown on the images. Note that these observations have various integration times. The markers are the same as those presented in Figure 4.

($282.061 \text{ mas yr}^{-1}$). In Table 6 we show the minimum time baseline required to find these stars, where we assume the star will be found when $D_{G,A,B} > a'' + b''$. MeerKAT has a similar astrometric precision to FIRST, so we have only included FIRST in the table. The astrometric precision values for SKA-low and SKA-mid are the resolutions listed in Braun *et al.* (2019). We can see from Table 6 that we would only require a time baseline of $\sim 0.6 \text{ yr}$ with the SKA-mid at 6.7 GHz to use this method to find a source with the same proper-motion as Sig CrB A. If we assume that SKA will be operational in 2030 then, of the eight proper-motion stars, BI Cet will have travelled the furthest since its J1998.8 FIRST detection: $\sim 0.0025 \text{ pc}$ ($8.3''$ at a distance of 62.12 pc). If we assume that

the minimum angular separation between the FIRST position of a source and the SKA 1.4 GHz position of a source is $1.4''$ then the maximum distance a source that travelled $\sim 0.0025 \text{ pc}$ could be detected at is $\sim 370 \text{ pc}$. This probes ~ 1.5 times the distance probed by FIRST-VLASS and ~ 4 times the distance probed by FIRST-RACS-mid. If we assume that the minimum angular separation between the FIRST position of a source and the SKA 6.7 GHz position of a source is $1.08''$ then the maximum distance a source that travelled $\sim 0.0025 \text{ pc}$ could be detected at is $\sim 480 \text{ pc}$. This probes ~ 2 times the distance probed by FIRST-VLASS and ~ 5 times the distance probed by FIRST-RACS-mid. Two sky surveys using SKA 6.7 GHz would probe to a similar distance

if the two surveys were performed ~ 4.5 yr apart, assuming that the sensitivity to stellar sources (taking into account radio spectral indices and SKA sensitivity at 6.7 GHz) is comparable to 1.4 GHz. Braun et al. (2019) suggests that the resolution of SKA-mid at 12.5 GHz will be $0.04''$. If we again assume that the sensitivity to stellar sources is comparable to 1.4 GHz, two surveys performed by SKA-mid at 12.5 GHz would probe to ~ 480 pc if the two surveys were performed ~ 2.5 yr apart. Even proper-motion matching between the lowest precision survey (RACS) and the highest precision survey (SKA-mid) requires less than 10 yr to find sources with similar proper-motions to sig CrB A. This demonstrates how the SKA will expand our searches for stellar radio sources. MeerKAT *L*-band observations have a similar astrometric accuracy to FIRST, which is important because MeerKAT is in the Southern hemisphere, compared to FIRST in the Northern hemisphere. This means that both RACS and MeerKAT will be key for providing the early-time observations to initially compare to SKA-mid.

The LOFAR Two-metre Sky Survey (LOTSS; Shimwell et al. 2017; Shimwell et al. 2022) catalogue does not currently provide the epoch of detection for each source because they revisit each field multiple times to achieve higher sensitivity and uv-coverage. However, for projects where proper-motion is important, it is key that epoch of detection/observation is provided. This can be done using an average epoch, similar to what is provided by FIRST, or by providing two catalogues: a catalogue of sources extracted from the deep/stacked images with no epoch provided, and a catalogue of sources extracted from single epoch observations with the epoch included. Many radio sources are persistent and extragalactic, which means that having accurate epoch information is not required for those sources.

It is now possible to perform large-scale searches for stellar radio sources (e.g. Pritchard et al. 2021; Callingham et al. 2021a) where proper-motion is important, plus searches for variable and transient radio sources (e.g. Variables and Slow Transients with ASKAP^d (VAST; Murphy et al. 2013), ThunderKAT^e (Fender et al. 2016)). We also need epoch information to account for sources with proper-motion when we are searching for variable and transient radio sources on long time scales. This is because we could identify a source as transient when it has just moved across the sky. This will be particularly important for high-resolution instruments such as the SKA and even current surveys with LOFAR, as the time baseline required for a star to move out of the position uncertainty region of its first detected position can be as small as $\lesssim 1$ yr. For example, two of the candidate radio variable stellar sources are the components of the binary system Wolf 424 (see Table 4). These stars have proper-motions magnitudes of 1.7 arcsec yr⁻¹ and 1.8 arcsec yr⁻¹. This means that they would be detected as two separate transients by VLASS, LOTSS and the SKA when comparing observations observed less than six months apart. Even with RACS, the survey with the highest position uncertainties, these stars would be identified as two radio transients in less than two years. Conversely, we may misidentify a transient source as extra-galactic if we do not account for the positions of stellar sources at each epoch. As such, we need to consider epoch information and how to appropriately include it in all current and future radio sky surveys and databases.

We found eight radio stellar sources using proper-motion searching, but we found 43 candidate variable stellar sources and

nine known radio stars (for a total of 52 sources, where five sources are likely chance coincidence) when we expanded our search to variable radio sources at ~ 1 400 MHz. The large number of variable sources compared to the small number of sources detected in two epochs implies that most stellar radio sources are detected because they flare, not because they are persistently bright in the radio. The area of the sky where RACS-mid and FIRST overlap is $-11.5 < \text{declination} < 49.5$ which gives a solid angle of ~ 20 000 deg². The six radio stellar sources found using FIRST-RACS-mid proper-motion searching range from ~ 22 to ~ 75 pc away, resulting in a surface density of 3×10^{-4} deg⁻² or a density of 2×10^{-9} pc⁻³. The 52 variable stellar sources (9 known and 43 candidate) range from ~ 30 to ~ 2 300 pc away, resulting in a surface density of 2.6×10^{-3} deg⁻² or a density of 2.6×10^{-10} pc⁻³. So while we probe deeper searching for variable stars, there is a higher number of stars per volume found using the proper-motion method.

This work demonstrates the star-finding power of performing high-resolution all sky radio surveys with radio interferometers. Even with a single all-sky survey per instrument we can find both proper-motion stellar sources and candidate variable radio stellar sources. However, we found many more candidate variable radio stellar sources than persistent proper-motion sources. BI Cet is an excellent example of why performing multi-epoch sky surveys is important for stellar searches. BI Cet has been observed multiple times by ASKAP as part of various surveys. We can see in Figure 6 that its brightness varies significantly in the different ASKAP epochs. If only one ASKAP sky survey was performed on J2020.05, BI Cet would not have been detected. This means some stars may be missed because they are faint/quiescent in one or both radio surveys. Specialist survey instruments such as ASKAP can survey the whole sky in a matter of weeks. Repeat sky surveys on various time baselines could assist in finding more stellar sources that are only sporadically radio bright.

Stokes V searches are biased towards coherent radio emission mechanisms; while variability searches are biased towards flaring stellar sources. Proper-motion searching only requires that the source is detected in two epochs. This means that it is biased towards sources that happened to flare in the two epochs or are persistently bright in the radio, but does not require further data on top of the radio continuum images and catalogues that are standard outputs of radio sky surveys. It also does not require a specific physical connection between the radio emission and the star to confirm that the star is the source of the radio emission. This is useful in reducing the biases in our searches for stellar radio sources. Combining the results of these search methods (Stokes V searches, variability searches, and proper-motion searches) is essential for finding as complete a sample of stellar radio sources as possible.

6. Conclusions

We have presented a method for identifying stellar radio sources using their proper-motion. We demonstrated this method using FIRST, VLASS, and RACS, and astrometric information from *Gaia* DR3; finding eight stellar radio sources, two of which had not previously been identified as radio stars. We also found 43 candidate variable radio stars and nine known radio stars by searching for sources that were detected in FIRST that are not detected in RACS-mid. Both of these methods will be important tools for identifying stellar radio sources as we perform sky surveys with

^d<https://www.vast-survey.org/>.

^e<http://www.thunderkat.uct.ac.za/>.

existing instruments and plan for sky surveys with the SKA. In particular, we should endeavour to include epoch information in radio sky survey catalogues and consider survey strategies where each pointing of the sky is observed more than once.

Acknowledgement. This scientific work uses data obtained from Inyarrimanha Ilgari Bundara/the Murchison Radio-astronomy Observatory. We acknowledge the Wajarri Yamaji People as the Traditional Owners and native title holders of the Observatory site. CSIRO's ASKAP radio telescope is part of the Australia Telescope National Facility. Operation of ASKAP is funded by the Australian Government with support from the National Collaborative Research Infrastructure Strategy. ASKAP uses the resources of the Pawsey Supercomputing Research Centre. Establishment of ASKAP, Inyarrimanha Ilgari Bundara, the CSIRO Murchison Radio-astronomy Observatory and the Pawsey Supercomputing Research Centre are initiatives of the Australian Government, with support from the Government of Western Australia and the Science and Industry Endowment Fund. This paper includes archived data obtained through the CSIRO ASKAP Science Data Archive, CASDA^f. This work has made use of data from the European Space Agency (ESA) mission *Gaia* (<https://www.cosmos.esa.int/gaia>), processed by the *Gaia* Data Processing and Analysis Consortium (DPAC, <https://www.cosmos.esa.int/web/gaia/dpac/consortium>).

Funding for the DPAC has been provided by national institutions, in particular the institutions participating in the *Gaia* Multilateral Agreement. This research made use of Astropy,^g a community-developed core Python package for Astronomy Astropy Collaboration *et al.* (2013, 2018). This research made use of APLpy, an open-source plotting package for Python Robitaille & Bressert (2012). This research has made use of the VizieR catalogue access tool, CDS, Strasbourg, France.^h The original description of the VizieR service was published in Ochsenbein, Bauer, & Marcout (2000). This research has made use of the SIMBAD database, operated at CDS, Strasbourg, (France Wenger *et al.* 2000). This research has made use of the CIRADA cutout service,ⁱ operated by the Canadian Initiative for Radio Astronomy Data Analysis (CIRADA). CIRADA is funded by a grant from the Canada Foundation for Innovation 2017 Innovation Fund (Project 35999), as well as by the Provinces of Ontario, British Columbia, Alberta, Manitoba and Quebec, in collaboration with the National Research Council of Canada, the US National Radio Astronomy Observatory and Australia's Commonwealth Scientific and Industrial Research Organisation. This research has made use of NASA's Astrophysics Data System Bibliographic Services.^j LND would like to acknowledge the traditional owners of the land where most of her work was performed: the Wurundjeri People of the Woi worrung Nation, the Whadjuk people of the Noongar Nation and the Gadigal people of the Eora Nation. We would like to thank the referee for their helpful comments.

Data Availability. All data used in this work are publicly available. ASKAP data can be accessed via the CSIRO ASKAP Science Data Archive (CASDA): <https://research.csiro.au/casda/>. FIRST data are available online: <http://sundog.stsci.edu/>. VLASS Quick Look data are available through CDS: <https://cdsarc.cds.unistra.fr/viz-bin/cat/J/ApJS/255/30>. *Gaia* DR3 data are publicly available from various data centres, data access is explained here: <https://www.cosmos.esa.int/web/gaia/data-access>.

Supplementary material. To view supplementary material for this article, please visit <https://doi.org/10.1017/pasa.2023.26>.

References

- Abazajian, K. N., *et al.* 2009, *ApJS*, **182**, 543
 Ahumada, R., *et al.* 2020, *ApJS*, **249**, 3
 Andersson, A., *et al.* 2022, *MNRAS*, **513**, 3482

- ASTROPY Collaboration, *et al.* 2013, *A&A*, **558**, A33
 ASTROPY Collaboration, *et al.* 2018, *AJ*, **156**, 123
 Babusiaux, C., *et al.* 2022, arXiv e-prints, arXiv:2206.05989
 Bailer-Jones, C. A. L., Rybizki, J., Foesneau, M., Demleitner, M., & Andrae, R. 2021, *AJ*, **161**, 147
 Becker, R. H., White, R. L., & Helfand, D. J. 1994, in *Astronomical Society of the Pacific Conference Series*, Vol. 61, *Astronomical Data Analysis Software and Systems III*, ed. D. R. Crabtree, R. J. Hanisch, & J. Barnes, 165
 Becker, R. H., White, R. L., & Helfand, D. J. 1995, *ApJS*, **450**, 559
 Becker, R. H., *et al.* 2001, *ApJS*, **135**, 227
 Bower, G. C., Bolatto, A., Ford, E. B., & Kalas, P. 2009, *ApJS*, **701**, 1922
 Bowler, B. P., *et al.* 2019, *ApJS*, **877**, 60
 Braun, R., Bonaldi, A., Bourke, T., Keane, E., & Wagg, J. 2019, arXiv e-prints, arXiv:1912.12699
 Callingham, J. R., Vedantham, H. K., Pope, B. J. S., Shimwell, T. W., & LoTSS Team. 2019, *RNAAS*, **3**, 37
 Callingham, J. R., *et al.* 2021, *NatAs*, **5**, 1233
 Camilo, F., *et al.* 2018, *ApJS*, **856**, 180
 Cook, N. J., *et al.* 2016, *MNRAS*, **457**, 2192
 Curiel, S., Ortiz-León, G. N., Mioduszewski, A. J., & Torres, R. M. 2020, *AJ*, **160**, 97
 Drake, S. A., Simon, T., & Linsky, J. L. 1986, *AJ*, **91**, 1229
 Driessen, L. N., *et al.* 2022, *MNRAS*, **510**, 1083
 Driessen, L. N., *et al.* 2020, *MNRAS*, **491**, 560
 Dulk, G. A. 1985, *ARA&A*, **23**, 169
 Fender, R., *et al.* 2016, in *MeerKAT Science: On the Pathway to the SKA*, ed. R. Taylor, F. Camilo, L. Leeuw, & K. Moodley, 13
 Flesch, E., & Hardcastle, M. J. 2004, *A&A*, **427**, 387
 Flesch, E. W. 2016, *PASA*, **33**, e052
 GAIA Collaboration, *et al.* 2016, *A&A*, **595**, A1
 Gordon, Y. A., *et al.* 2021, *ApJS*, **255**, 30
 Hale, C. L., *et al.* 2021, *PASA*, **38**, e058
 Helfand, D. J., Schnee, S., Becker, R. H., White, R. L., & McMahon, R. G. 1999, *AJ*, **117**, 1568
 Helfand, D. J., White, R. L., & Becker, R. H. 2015, *ApJ*, **801**, 26
 Hewett, P. C., Foltz, C. B., & Chaffee, F. H. 2001, *AJ*, **122**, 518
 Hotan, A. W., *et al.* 2021, *PASA*, **38**, e009
 Jones, D. L., Lestrade, J.-F., Preston, R. A., & Phillips, R. B. 1995, in *Astronomical Society of the Pacific Conference Series*, Vol. 74, *Progress in the Search for Extraterrestrial Life*, ed. G. S. Shostak, 219
 Kervella, P., Arenou, F., Mignard, F., & Thévenin, F. 2019, *A&A*, **623**, A72
 Kimball, A. E., *et al.* 2009, *ApJ*, **701**, 535
 Kozhevnikova, A. V., & Alekseev, I. Y. 2015, *ARep*, **59**, 937
 Lacy, M., *et al.* 2020, *PASP*, **132**, 035001
 Lestrade, J.-F., Jones, D. L., Preston, R. A., & Phillips, R. B. 1994, *Ap&SS*, **212**, 251
 Lestrade, J.-F., Niell, A. E., Preston, R. A., & Mutel, R. L. 1988, *AJ*, **96**, 1746
 Lestrade, J.-F., Phillips, R. B., Preston, R. A., & Gabuzda, D. C. 1992, *A&A*, **258**, 112
 Lestrade, J. F., *et al.* 1999, *A&A*, **344**, 1014
 Luck, R. E. 2015, *Aj*, **150**, 88
 McConnell, D., *et al.* 2020, *PASA*, **37**, e048
 McMahon, R. G., White, R. L., Helfand, D. J., & Becker, R. H. 2002, *ApJS*, **143**, 1
 Morris, D. H., & Mutel, R. L. 1988, *Aj*, **95**, 204
 Murphy, T., *et al.* 2013, *PASA*, **30**, e006
 Ochsenbein, F., Bauer, P., & Marcout, J. 2000, *A&AS*, **143**, 23
 Osten, R. A. 2008, arXiv e-prints, arXiv:0801.2573
 Perley, R. A., Chandler, C. J., Butler, B. J., & Wrobel, J. M. 2011, *ApJ*, **739**, L1
 Pritchard, J., *et al.* 2021, *MNRAS*, **502**, 5438
 Robitaille, T., & Bressert, E. 2012, APLpy: Astronomical Plotting Library in Python, *Astrophysics Source Code Library*, ascl:1208.017
 Samus', N. N., Kazarovets, E. V., Durevich, O. V., Kireeva, N. N., & Pastukhova, E. N. 2017, *ARep*, **61**, 80
 Shimwell, T. W., *et al.* 2017, *A&A*, **598**, A104
 Shimwell, T. W., *et al.* 2022, *A&A*, **659**, A1
 Simon, T., Fekel, F. J., & Gibson, D. M. 1982, in *BAAS*, **14**, 982

^f<http://data.csiro.au/>.

^g<http://www.astropy.org>.

^h10.26093/cds/vizieR.

ⁱ<http://cutouts.cirada.ca/>.

^j<https://ui.adsabs.harvard.edu/>.

- Spangler, S. R., Owen, F. N., & Hulse, R. A. 1977, *Aj*, **82**, 989
- Spangler, S. R., Shawhan, S. D., & Rankin, J. M. 1974, *ApJ*, **190**, L129
- Strassmeier, K. G., Weber, M., Granzer, T., & Järvinen, S. 2012, *AN*, **333**, 663
- Toet, S. E. B., et al. 2021, *A&A*, **654**, A21
- Vallenari, A., et al. 2022, Gaia DR3 documentation Chapter 19: Performance verification, Gaia DR3 documentation, European Space Agency; Gaia Data Processing and Analysis Consortium. Online at <https://gea.esac.esa.int/archive/documentation/GDR3/index.html>, id. 19
- van Haarlem, M. P., et al. 2013, *A&A*, 556, doi: [10.1051/0004-6361/201220873](https://doi.org/10.1051/0004-6361/201220873)
- Vedantham, H. K., et al. 2022, *ApJ*, **926**, L30
- Wendker, H. J. 1995, *A&AS*, **109**, 177
- Wenger, M., et al. 2000, *A&ASS*, **143**, 9